Low-Complexity N-port ADCs Using 2-D Δ-Σ Noise-Shaping for N-Element Array Receivers

A. Nikoofard*, J. Liang*, M. Twieg†, S. Handagala‡, A. Madanayake‡, L. Belostotski§, S. Mandal*
*Electrical Engineering and Computer Science Department, Case Western Reserve University, Cleveland, Ohio 44106
†Radiology Department, Case Western Reserve University, Cleveland, Ohio 44106
‡Electrical and Computer Engineering Department, University of Akron, Akron, Ohio 44325
§Electrical and Computer Engineering Department, University of Calgary, Calgary, AB, Canada
Email: {axn285, jxl1265, mdt24}@case.edu, surangahandagala@gmail.com, arjuna@uakron.edu,
lbelosto@ucalgary.ca, sxm833@case.edu

***Abstract*—A novel multi-dimensional noise-shaping method is proposed to extend Δ-Σ modulation to the two-dimensional (2-D) (space, time) case. It uses spatial oversampling to provide another degree of freedom for ADC designers to shape quantization noise when temporal oversampling is limited. The method uses lossless discrete integrators (LDIs) to implement spatial integrators and is suitable for use in microwave and mm-wave array processing systems. The resulting 2-D noise shaping reduces the spectral overlap of a desired array signal with that of quantization noise. Shaped noise can then be removed from the region of support (ROS) of the array signal using 2-D filtering, thus improving the overall signal-to-quantization noise ratio (SQNR) and effective number of bits (ENOB). Simulation results from an integrated 64-channel converter in UMC 65nm CMOS prove the functionality of the approach. Experimental results from a board-level 64-channel converter are also presented.**

I. Introduction

Digital antenna arrays that perform beamforming are essential for wireless communications, imaging, and radar. Modern receivers for N-element arrays independently process input signals from each antenna element in the aperture. However, this approach is not optimal because it does not consider the relationships that must exist between received signals, additive noise, various forms of interference, and non-linear distortion across the array [1]. Specifically, Special Relativity defines a region of causality (i.e., the light cone) outside which no propagating electromagnetic waves can exist. This fact has the potential to greatly improve the performance of array processors. Specifically, spatially-oversampled arrays can be used to i) compress the light cone of the input signals (i.e., their region of support (ROS)) such that it occupies a smaller portion of the 2-D (space, time) frequency domain; and ii) spectrally shape the noise and distortion stemming from practical amplifiers, mixers, and data converters, such that they do not overlap with the compressed light cone (see Fig. 1(a)). We call this approach "spatio-temporal noise shaping" [2]. It is conceptually similar to Δ-Σ modulation, but extended to the 2-D spatio-temporal domain. This approach results in lower thermal noise, higher amplifier and mixer linearity, and higher data converter resolution (ENOB) than conventional array design approaches in which noise, distortion, and the signal of interest overlap in the 2-D frequency domain.

Instead of using N independent complex (I/Q) ADCs for an N-element array receiver, the proposed multi-port ADC digitizes the array signal in a single spatiotemporal quantization operation that takes into account the finite speed of light and the resultant light cone. This "array digitization" approach decreases power consumption by enabling the quantization noise to be shaped in multiple dimensions (e.g., along space x, y and time t for a rectangular array) to be dominantly outside the spatio-temporal frequency domain ROS of the array signal. The shaped noise is later removed from the digitized outputs by a spatial low-pass filter (such as a phased-array or true-time-delay beamformer). As a result, the proposed approach promises significant improvements in the power efficiency of array ADCs. This is important because ADC power consumption is the dominant factor for array processing operations such as dynamic beam-forming since it grows exponentially with resolution, i.e., as 2^b for b bits.

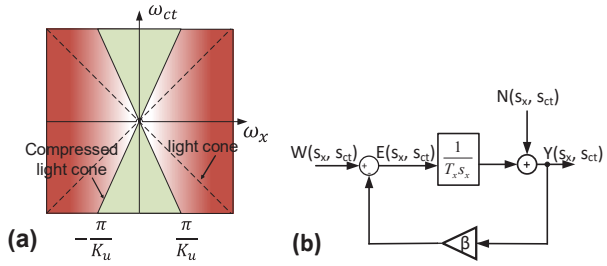

Fig. 1. (a) The ROS of electromagnetic waves received by a spatially-oversampled antenna array (green) consists of a compressed light cone. Spatial sigma-delta noise-shaping ensures that receiver noise and distortion (red) lies outside the ROS of the received signals. (b) Continuous frequency domain representations of a first-order spatial Δ-Σ modulator.

II. Δ-Σ Space-Time Noise Shaping

Fig. 1(b) shows the block diagram of a continuous-time first-order spatial Δ-Σ modulator. Here $w(x, ct)$ denotes the input signal at spatial location x and time t where c is the speed of light, while $W(s_x, s_{ct})$ denotes the signal in the 2-D Laplace domain. Similarly y and Y refer to the outputs in the space-time and transform domains, respectively. Also, $n(x, ct)$ and $N(s_x, s_{ct})$ denote noise in these domains.

Analyzing Fig. 1(b) in the 2-D Laplace domain gives

$$Y(s_x, s_{ct}) = \frac{W(s_x, s_t)}{\beta + T_x s_x} + N(s_x, s_{ct}) \frac{T_x s_x}{\beta + T_x s_x}. \quad (1)$$

Hence the signal is low-pass filtered while the noise is high-pass filtered, thus reducing the overlap between them. However, the system described in (1) is unrealizable because in practice antenna elements have to be placed in a spatially discrete manner. In particular, the inter-antenna spacing for uniform linear arrays is $\Delta x = \lambda / (2K_x)$ where λ is the wavelength of the highest-frequency signal of interest and

$K_x \geq 1$ is the spatial oversampling factor relative to a Nyquist-sampled array with spacing of $\lambda/2$. As a result, the spatial dimension is always discretized such that $x = n_x \Delta x$, which results in a z-transform variable $z_x \in \mathbb{C}$ for the spatial transform domain in place of the Laplace variable $s_x \in \mathbb{C}$. The necessary $s_x \rightarrow z_x$ transformation cannot use the well-known bilinear transform operator $s_x = \frac{1-z_x^{-1}}{1+z_x^{-1}}$ because it results in a delay-free loop, which makes the algorithm uncomputable. Fortunately, it can be shown that a modified lossless discrete integrator (LDI) with the transformation $\frac{1}{T_x s_x} = \frac{1}{\beta} \frac{1}{1-z_x^{-1}}$ can overcome delay-free loops, making this a viable candidate for spatially-discrete realizations. The resulting system is given by

$$Y(z_x, s_{ct}) = \frac{1}{\beta} W(z_x, s_{ct}) + (1 - z_x^{-1}) N(z_x, s_{ct}). \quad (2)$$

The signal transfer function shows that the input is amplified by the ADC transfer function $A = 1/\beta$. However, the quantization noise gets shaped by the first-order spatial high pass filter $\left(1 - z_x^{-1}\right)$. Practical N-port ADC array architectures can thus be realized by using this topology.

III. N-PORT Δ-Σ ADC

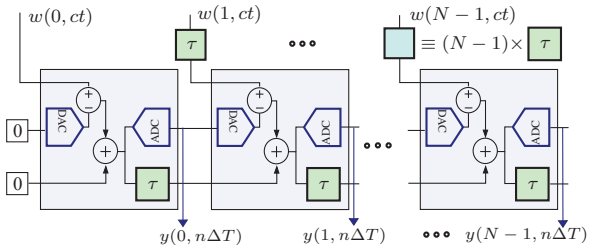

Fig. 2. Structure of the proposed N-port Δ-Σ ADC. Each shaded block denotes a single spatial integration and amplification module (SIAM).

The transfer function in (2) defines a signal flow graph that is implemented by using a so-called spatial integration and amplification module (SIAM). Each SIAM (see Fig. 2) contains a b-bit quantizer (denoted as ADC), a b-bit DAC, two summing junctions, and optional analog time delays (denoted by τ) that compensate for time delay within the quantizer. The latter are not used here; if necessary, they can be implemented using all-pass filters. Feed-forward interconnection of N SIAMs results in a N-input, N-output system, as shown in Fig. 2. This structure, which achieves 2-D Δ-Σ noise shaping, forms the basis for the ADCs considered in this paper.

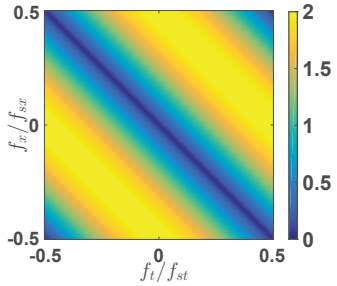

Fig. 3. 2-D (space,time) noise-shaping function for the N-port ADC.

We first analyze conventional 1-D noise-shaping. Assuming K_u as the oversampling ratio and N-th order noise-shaping, the quantization noise is high-pass filtered by the discrete-time transfer function $H(z) = \left(1 - z^{-1}\right)^N$ where

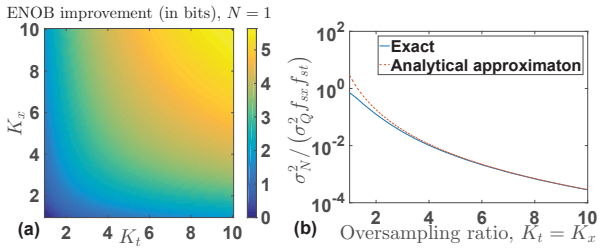

Fig. 4. (a) Normalized quantization noise improvement (in bits) due to time-space over-sampling. (b) Comparison of exact and approximate expressions for quantization noise when $K_t = K_x$. In both cases, $N = 1$.

$z = e^{-j\omega T_s}$, $\omega = 2\pi f$, and $f_s = 1/T_s$ is the sampling frequency. The corresponding continuous-time function is $H(f) = \left(1 - e^{-j2\pi f T_s}\right)^N$, resulting in a noise variance of

$$\sigma_N^2 = \frac{\sigma_Q^2 2^{2N}}{2\pi T_s} \int_0^{\pi/K_u} \sin^{2N}(\theta/2) d\theta. \quad (3)$$

where σ_Q^2 is the power spectrum density (PSD) of quantization noise, and $\theta \equiv 2\pi f T_s$. To get insight into (3), assume large oversampling, i.e., $fT_s \ll 1$. Now $\sin(\theta/2) \approx \theta/2$, so

$$\frac{\sigma_N^2}{\sigma_Q^2} = \frac{f_s}{2\pi} \int_0^{\pi/K_u} \theta^{2N} d\theta = \left(\frac{\pi}{K_u}\right)^{2N+1} \frac{f_s}{2\pi\,(2N+1)}. \quad (4)$$

Eqn. (4) shows that to reduce quantization noise, one may increase either K_u or N. Specifically, the noise variance decreases as $K_u^{-(2N+1)}$. Now we consider the proposed 2-D approach. Using similar methods, the noise variance is

$$\sigma_N^2 = \sigma_Q^2 \int_0^{f_s/2K_x} \int_0^{f_s/2K_t} |F(f_x, f_t)|^{2N} df_x df_t, \quad (5)$$

where K_x and K_t are the spatial and temporal oversampling ratios, respectively, and $F(z_x, z_t)$ is the corresponding 2-D noise shaping function. Analyzing the system in Fig. 2 with a one-clock-cycle quantizaton time delay results in $F(z_x, z_t) = \left(1 - {z_x}^{-1} {z_t}^{-1}\right)$. The continuous-domain version is

$$F(f_x, f_t) = 1 - \exp(-j2\pi f_x/f_{sx}) \exp(-j2\pi f_t/f_{st}), \quad (6)$$

where f_{sx} and f_{st} are the spatial and temporal sampling frequencies, respectively. This function is shown in Fig. 3. Defining $\theta_1 = 2\pi f_x/f_{sx}$ and $\theta_2 = 2\pi f_t/f_{st}$, (6) becomes

$$\frac{{\sigma^2}_N}{{\sigma^2}_Q} = \frac{f_{sx} f_{st} 2^{2N}}{4\pi^2} \int_0^{\pi/K_x} \int_0^{\pi/K_t} \sin^{2N}\left(\frac{\theta_1 + \theta_2}{2}\right) d\theta_1 d\theta_2. \quad (7)$$

Eqn. (7) can be solved numerically. Fig. 4(a) shows the improvement in signal-to- quantization noise ratio (SQNR) due to oversampling in both domains for $N = 1$. To get design insight, we assume large oversampling in both dimensions such that $\sin((\theta_1 + \theta_2)/2) \approx (\theta_1 + \theta_2)/2$. The result is

$$\frac{{\sigma^2}_N}{{\sigma^2}_Q} = W\left(\left(\frac{1}{K_t} + \frac{1}{K_x}\right)^{2N+2} - \frac{1}{{K_t}^{2N+2}} - \frac{1}{{K_x}^{2N+2}}\right), \quad (8)$$

where $W = f_{sx} f_{st} (\pi)^{2N+2} / \left(4\pi^2 (2N+1)(2N+2)\right)$. Fig. 4(b) compares this expression with the exact solution for the $K_t = K_x$ case, and shows that it is an excellent approximation for oversampling ratios > 3. The symmetric nature of (8), which ultimately arises from the symmetric form

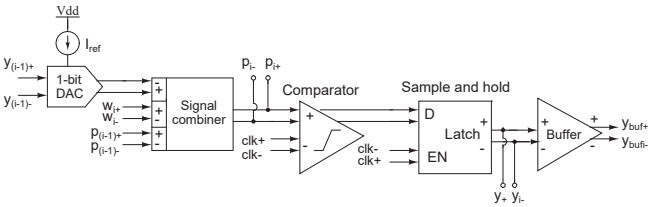

Fig. 5. Block diagram of a SIAM for the integrated 2D noise-shaping ADC.

of $F(z_x, z_t)$, shows that oversampling in either dimension has the same effect on SQNR. Moreover, the fact that spatial and temporal oversampling can be combined to further improve SQNR shows that the proposed 2-D noise-shaping method provides another degree of freedom for the ADC designer.

IV. Simulation Results

A prototype 64-channel noise-shaping ADC using 1-bit quantization has been designed in the UMC 65nm CMOS process for mm-wave beamforming applications. It uses source-coupled logic (SCL) in order to optimize the trade-off between propagation delay, switching speed, and power consumption. SCL gates are based on switching current in differential pairs, which results in fully-differential designs with controllable voltage swing [3]. The schematic of a single channel (i.e., SIAM) within the preliminary implementation of a N-port ADC using 1-bit quantization is shown in Fig. 5. The circuit implements the signal flow graph shown in Fig. 2. Foundry-provided macromodels that include layout parasitics were used for both the transistors and passive components in order to improve simulation accuracy. The key blocks within each SIAM include input and output buffers, a signal combiner, a comparator, and another buffer that acts as a 1-bit DAC. The signal combiner performs spatial integration by acting as a soft OR-gate. It was implemented in current-mode as shown in Fig. 6(a). A feedback loop based on a replica bias circuit (not shown) ensures that the effective voltage gain of each signal within the combiner is close to unity, which is necessary for spatial filtering of the quantization noise. The full-scale voltage V_{FS} is set by the 1-bit DAC; its maximum value is limited by the linear range of the signal combiner. The comparator consists of a linear preamplifier that uses shunt-peaking with on-chip inductors to increase bandwidth [4] followed by an SCL latch (see Fig. 6(b)). The preliminary implementation has not been optimized for power; it consumes 20mW per channel.

We tested the converter by generating broadband plane wave input signals corresponding to various arrival angles that were then coherently downconverted to baseband. The simulations used $V_{FS} = 0.21$V and oversampling ratios of $K_x = K_t = 4$. The resulting SQNR for a full-scale input with a double-sided bandwidth of 1GHz (which is typical for a mm-wave communication signal) was 29.0 dB at a clock frequency of $f_{clk} = 4$ GHz. This result corresponds to an effective number of bits (ENOB) of 4.5, which is sufficient for many mm-wave communication scenarios [5], [6]. It is also in good agreement with Fig. 4(a), which predicts ENOB = 4.1. Note that the addition of spatial oversampling improves ENOB by ~ 2.0 bits relative to its value for temporal oversampling alone. The simulated spatial output spectrum of the converter is shown in Fig. 7 for two different arrival angles. Smaller input

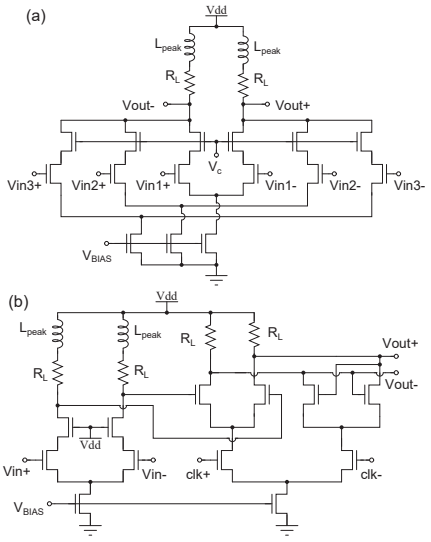

Fig. 6. Schematic of the (a) signal combiner and (b) comparator.

signals (10% of full-scale) were used here to highlight the quantization noise, which is clearly spatially high-pass filtered.

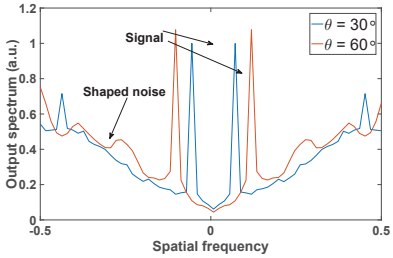

Fig. 7. Simulated spatial output spectra of a 64-port ADC with first-order noise-shaping for 10% full-scale inputs at two different arrival angles.

Our preliminary results correspond to a Walden figure-of-merit [7] of 0.87pJ/bit. In addition, simulations indicate typical digital rise and fall times of ≈40ps. As a result, f_{clk} can be as high as 10GHz, which corresponds to a temporal oversampling ratio of $K_t = 10$. As a result, ENOB should be further improved by 1.1 bits, corresponding to an FOM of 0.41pJ/bit, which is competitive with the state-of-the-art in this sampling frequency range. Further FOM improvements are likely through circuit optimization. Larger spatial oversampling ratios are obviously also helpful, but in practice K_x is limited by the physical sizes of the antennas and their mutual coupling.

V. Experimental Results

We also have designed and tested a low-speed ($f_s < 40$MHz) discrete board-level converter based on 1-bit quantization. A simplified schematic of the circuit, which uses off-the-shelf components, is shown in Fig. 9. High-speed operational amplifiers (op-amps) are used to realize the signal combiner and all-pass filter (for canceling the ∼7ns comparator propagation delay), while the 1-bit DAC is realized using an analog multiplexer. The top of Fig. 10 shows the entire 64-channel converter, which uses four identical boards, while the bottom shows one board containing 16 identical channels. The entire system draws 1.59A and 1.02A from +7V and -6V

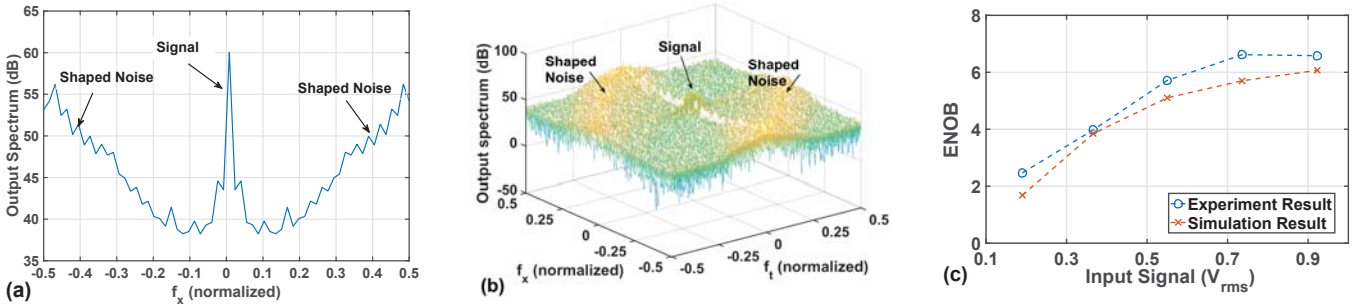

Fig. 8. (a) Measured noise-shaped 2-D output spectrum of the 64-channel ADC when f_s is 11.4 MHz and the input signal amplitude is 0.19V_{rms}. (b) Measured noise-shaped 3-D output spectrum for the same measurement conditions as (a). (c) Relationship between ENOB and input signal amplitude.

power supplies, respectively. The core circuits run on $\pm$5V supplies generated by on-board linear voltage regulators.

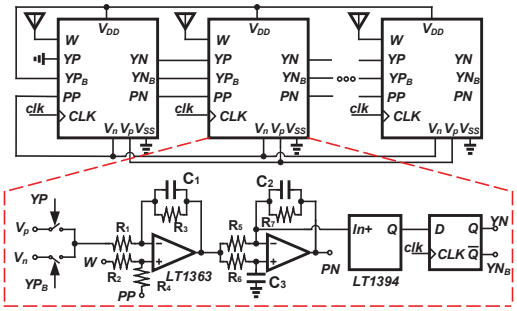

Fig. 9. An N-port ADC with first-order noise-shaping realized using discrete off-the-shelf components. $R_1 = R_2 = R_3 = R_4 = R_5 = R_7 = 1\text{k}\Omega$, $R_6 = 330\Omega$, $C_1 = 5.3$pF, $C_2 = 22$pF, and $C_3 = 100$pF.

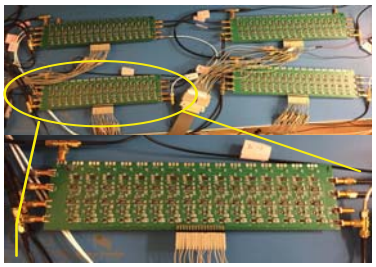

Fig. 10. Photograph of the 64-channel noise-shaping ADC realized using 4 boards. Each board contains 16 identical channels.

During the experiments we used a broadband input signal with the bandwidth of 500 kHz that was buffered and then applied to the inputs of all the channels. This input was chosen to simulate a typical wireless communications scenario. It corresponds to an amplitude- and phase-modulated plane wave at perpendicular incidence to the array (arrival angle =0°) after amplification and downconversion to baseband by conventional heterodyne receivers connected to each antenna. Fig. 8(a) shows the measured noise-shaped 2-D output spectrum of the ADC when the sampling frequency f_s is 11.4 MHz (temporal oversampling ratio $K_t = 11.4$) and the input signal amplitude is 0.19V_{rms} ($\sim 1\text{V}_{pp}$). Only one peak at zero spatial frequency is obtained since the input signal has 0° arrival angle. We assume that the antennas are spaced to obtain a spatial oversampling ratio $K_x = 4$. The resulting normalized signal bandwidth is $\pm 0.5/K_x = \pm 0.125$. It is evident that the noise is shaped out of this spectral region, as expected. Fig. 8(b) shows the measured 3-D output spectrum from the same measurement conditions as Fig. 8(a). This figure proves that the measured 2-D noise shaping function is in excellent agreement with the theory (shown in Fig. 3).

Fig. 8(c) shows the simulated and measured ENOB of the converter versus input amplitude. ENOB increases linearly with amplitude until approximately 0.73V_{rms} ($\sim 4\text{V}_{pp}$) before starting to decrease. This is because input signals $> 0.73\text{V}_{rms}$ contain excursions that exceed the linear range of the op-amps. The resulting maximum ENOB is 6.6, which is in excellent agreement with the simulations. It is also in good agreement with the theoretical prediction of 5.3 (shown in Fig. 4(a)).

VI. Conclusion

This paper has proposed a new method for shaping the quantization noise of multi-channel Δ-Σ ADCs in 2-D (both time and space). By employing antenna arrays and taking advantage of oversampling the input signal in both dimensions, we have shown that the resolution of the ADC can be significantly improved. Mathematical analysis, simulations, and experimental results prove the functionality of the proposed method. Future work will focus on higher-order noise-shaping.

References

[1] N. Liyanage, L. Bruton, and P. Agathoklis, "On the attenuation of interference and mutual coupling in antenna arrays using 3d space-time filters," in *2009 IEEE Pacific Rim Conference on Communications, Computers and Signal Processing*, Aug 2009, pp. 146–151.

[2] S. Handagala, A. Madanayake, L. Belostotski, and L. T. Bruton, "Δ-Σ noise shaping in 2D space-time for uniform linear aperture array receivers," in *IEEE Moratuwa Engg. Research Conf. (MERCon)*, 2016.

[3] M. Alioto and G. Palumbo, "Design strategies for source coupled logic gates," *IEEE Transactions on Circuits and Systems I: Fundamental Theory and Applications*, vol. 50, no. 5, pp. 640–654, May 2003.

[4] S. Shekhar, J. S. Walling, and D. J. Allstot, "Bandwidth extension techniques for CMOS amplifiers," *IEEE Journal of Solid-State Circuits*, vol. 41, no. 11, pp. 2424–2439, Nov 2006.

[5] R. Narasimha, M. Lu, N. R. Shanbhag, and A. C. Singer, "BER-optimal analog-to-digital converters for communication links," *IEEE Transactions on Signal Processing*, vol. 60, no. 7, pp. 3683–3691, July 2012.

[6] O. Orhan, E. Erkip, and S. Rangan, "Low power analog-to-digital conversion in millimeter wave systems: Impact of resolution and bandwidth on performance," in *Information Theory and Applications Workshop (ITA), 2015*, Feb 2015, pp. 191–198.

[7] R. H. Walden, "Analog-to-digital converter survey and analysis," *IEEE J. Selected Areas in Comms.*, vol. 17, no. 4, pp. 539–550, Apr 1999.